https://doi.org/10.5194/tc-2019-334
Preprint. Discussion started: 14 January 2020

The Cryosphere Discussions

ISMIP6 projections of ocean-forced Antarctic Ice Sheet evolution using the Community Ice Sheet Model

William H. Lipscomb[1], Gunter R. Leguy[1], Nicolos C. Jourdain[2], Xylar Asay-Davis[3], Hélène Seroussi[4], and Sophie Nowicki[5]

[1]Climate and Global Dynamics Laboratory, National Center for Atmospheric Research, Boulder, CO, USA
[2]Univ. Grenoble Alpes/CNRS/IRD/G-INP, IGE, Grenoble, France
[3]Los Alamos National Latoratory, Los Alamos, NM, USA
[4]Jet Propulsion Laboratory, California Institute of Technology, Pasadena, CA, USA
[5]NASA Goddard Space Flight Center, Greenbelt, MD, USA

Correspondence: William H. Lipscomb (lipscomb@ucar.edu)

Abstract. The future retreat rate for marine-based regions of the Antarctic Ice Sheet is one of the largest uncertainties in sea-level projections. The Ice Sheet Model Intercomparison Project for CMIP6 (ISMIP6) aims to improve projections and quantify uncertainties by running an ensemble of ice sheet models with atmosphere and ocean forcing derived from global climate models. Here, ISMIP6 projections of ocean-forced Antarctic Ice Sheet evolution are illustrated using the Community Ice Sheet Model (CISM). Using multiple combinations of sub-ice-shelf melt parameterizations and calibrations, CISM is spun up to steady state over many millennia. During the spin-up, basal friction parameters and basin-scale thermal forcing corrections are adjusted to nudge the ice thickness toward observed values. The model is then run forward for 500 years, applying ocean thermal forcing anomalies from six climate models. In all simulations, the ocean forcing triggers long-term retreat of the West Antarctic Ice Sheet, including the Amundsen, Filchner-Ronne, and Ross Basins. Mass loss accelerates late in the 21st century and rises steadily over the next several centuries without leveling off. The resulting ocean-forced SLR at year 2500 varies from about 10 cm to nearly 2 m, depending on the melt scheme and model forcing. Relatively little ice loss is simulated in East Antarctica. Large uncertainties remain, as a result of parameterized basal melt rates, missing ocean and ice sheet physics, and the lack of ice–ocean coupling.

1 Introduction

The Antarctic Ice Sheet has been losing mass at an increasing rate for the past several decades (Shepherd et al., 2018; Rignot et al., 2019). Much of the ice loss has been driven by increased access of warm Circumpolar Deep Water to marine-based parts of the West Antarctic Ice Sheet (WAIS), likely caused in part by radiatively forced changes in wind patterns (Thomas et al., 2004; Jenkins et al., 2010; Rignot et al., 2013; Holland et al., 2019). Paleoclimate records show that the WAIS retreated in past climates not much warmer than the present, including the Last Interglacial (Dutton et al., 2015). Many WAIS glaciers lie on reverse-sloping beds (i.e., with the seafloor sloping upward in the direction of ice flow), making these glaciers vulnerable to the marine ice sheet instability (MISI; Weertman, 1974; Mercer, 1978; Schoof, 2007). Models suggest that ice in the Amundsen

https://doi.org/10.5194/tc-2019-334
Preprint. Discussion started: 14 January 2020

Sea sector, including Thwaites and Pine Island Glaciers, may already be in the early stages of collapse (Joughin et al., 2014; Favier et al., 2014). Despite recent advances in ice sheet modeling (Pattyn, 2018), projections of 21st century Antarctic Ice Sheet retreat and resulting sea-level rise (SLR) are highly uncertain, ranging from modest ($\sim$ 10 cm; Ritz et al., 2015) to large and abrupt ($>$ 1 m; Pollard and DeConto, 2016). Although recent work (Edwards et al., 2019) suggests that the most extreme projections may overestimate the rate of SLR, much of the WAIS is likely vulnerable to long-term, self-sustaining retreat.

To improve projections and better understand and quantify uncertainties, ice sheet modelers have organized several community intercomparisons, most recently the Ice Sheet Model Intercomparison Project for CMIP6 (ISMIP6; Nowicki et al., 2016). ISMIP6 has been endorsed by the Coupled Model Intercomparison Project – Phase 6 (CMIP6; Eyring et al., 2016) and is providing process-based ice-sheet and sea-level projections linked to the CMIP ensemble of climate projections from atmosphere–ocean general circulation models (AOGCMs). Nowicki et al. (in review) have summarized the ISMIP6 projection protocols for standalone ice sheet model (ISM) experiments. The general strategy is to use outputs from CMIP5 and CMIP6 climate models to derive atmosphere and ocean fields for forcing ISMs over the period 2015–2100. Goelzer et al. (in review) and Seroussi et al. (in review) have evaluated the multi-model ensembles of projections for the Greenland and Antarctic Ice Sheets, respectively.

Seroussi et al. (in review) analyzed 18 sets of Antarctic simulations from 15 international groups, with forcing derived from six CMIP5 AOGCMs and representing a spread of climate model results. The Antarctic contribution to sea level during 2015–2100 varies from sea-level fall of 7.8 cm to sea-level rise of 30.0 cm under the RCP (Representative Concentration Pathway) 8.5 scenario. The main contributor to falling sea level is a more positive surface mass balance (SMB), with several AOGCMs simulating more snowfall in a warming climate. Antarctic SLR, on the other hand, is driven by ocean warming leading to marine ice-sheet retreat and dynamic mass loss, especially for WAIS. The amount of ice loss varies widely across simulations because of differences in the strength and spatial patterns of AOGCM ocean warming, and in ISM physics and numerics.

This paper aims to complement the study of Seroussi et al. (in review) by evaluating the Antarctic response to ocean forcing in a single model, the Community Ice Sheet Model (CISM; Lipscomb et al., 2019). We do not simulate atmospheric forcing changes, since the ice-sheet response to SMB anomalies is relatively consistent across models for both Greenland (Goelzer et al., in review) and Antarctica (Seroussi et al., 2019). This is not to say that SMB changes are unimportant for future Antarctic Ice Sheet evolution, only that the SMB contribution is less uncertain than the ocean contribution. Instead, we consider the Antarctic Ice Sheet response to increased sub-ice-shelf melting as a function of basal melting parameterizations (Jourdain et al., in review) and AOGCM ocean warming. To study long-term ice sheet evolution, we extend the simulations to 2500, with the forcing after 2100 based on late-21st forcing from high-end emissions scenarios. In this way, we explore the following questions:

- If the ocean warming projected for the late 21st century were to continue unabated for several more centuries, what parts of the Antarctic Ice Sheet would be most vulnerable to retreat?
- Given this vulnerability, and assuming that emissions remain on a high-end trajectory until 2100, what will be the committed amount of long-term, ocean-forced sea-level rise from Antarctic ice loss?

https://doi.org/10.5194/tc-2019-334
Preprint. Discussion started: 14 January 2020

Rather than make quantitative predictions (which remain elusive because of model and forcing uncertainties), our main intent is to explore parameter space, taking advantage of the ISMIP6 framework to build on previous multi-century Antarctic simulations (e.g., Pollard and Deconto, 2009; Cornford et al., 2015; Pollard and DeConto, 2016; Larour et al., 2019). The ice-sheet physics is conventional in the sense that it includes well-understood retreat mechanisms such as MISI, but not hydrofracture or cliff collapse (Pollard et al., 2015; Pollard and DeConto, 2016). Some important long-term feedbacks such as solid-Earth rebound and relative-sea-level changes (Gomez et al., 2010; Larour et al., 2019) are omitted, and there is no ice–ocean coupling (e.g., De Rydt and Gudmundsson, 2016; Seroussi et al., 2017; Favier et al., 2019). Thus, the timing and magnitude of simulated ice sheet retreat are imprecise, but we can identify responses that are robust across simulations, and also draw attention to the largest sources of uncertainty.

Section 2 gives an overview of CISM and summarizes the protocol and ocean data sets for ISMIP6 Antarctic projections. We describe the model initialization technique and evaluate the spun-up state in Sect. 3, and we present the results of ocean-forced simulations in Sect. 4. Section 5 gives conclusions and suggests directions for future research.

2 Model and experimental description

2.1 The Community Ice Sheet Model

The Community Ice Sheet Model (CISM) is a parallel, higher-order ice sheet model designed to perform continental-scale simulations on timescales of decades to millennia. CISM is a descendant of the Glimmer model (Rutt et al., 2009) and is now an open-source code developed mainly at the National Center for Atmospheric Research, where it serves as the dynamic ice sheet component of the Community Earth System Model (CESM). The most recent documented release was CISM v2.1 (Lipscomb et al., 2019), coinciding with the 2018 release of CESM2 (Danabasoglu et al., in review). The model performs well for community benchmark experiments, including the ISMIP-HOM experiments for higher-order models (Pattyn et al., 2008) and several stages of the Marine Ice Sheet Model Intercomparison Project: the original MISMIP (Pattyn et al., 2012), MISMIP3d (Pattyn et al., 2013), and MISMIP+ (Asay-Davis et al., 2016; Cornford et al., in review). CISM participated in two earlier ISMIP6 projects focused on ice sheet model initialization: initMIP-Greenland (Goelzer et al., 2018) and initMIP-Antarctica (Seroussi et al., 2019). More recently, CISM results were submitted for the ISMIP6 projections (Goelzer et al., in review; Seroussi et al., in review), the LARMIP-2 experiments (Levermann et al., 2019), and the Antarctic BUttressing Model Intercomparison Project (ABUMIP; Sun et al., in review).

CISM runs on a structured rectangular grid with a terrain-following vertical coordinate. The simulations in this paper were run on a 4-km grid with 5 vertical levels, as for the CISM contributions to ISMIP6 projections (Seroussi et al., in review). Scalars (e.g., ice thickness H and temperature T) are located at grid cell centers, with horizontal velocity $\boldsymbol{u} = (u, v)$ computed at vertices. The dynamical core has parallel solvers for a hierarchy of approximations of the Stokes ice-flow equations, including the shallow-shelf approximation (MacAyeal, 1989), a depth-integrated higher-order approximation (Goldberg, 2011), and the 3D Blatter-Pattyn higher-order approximation (Blatter, 1995; Pattyn, 2003). (The latter two approximations are classified as

https://doi.org/10.5194/tc-2019-334
Preprint. Discussion started: 14 January 2020


The Cryosphere Discussions

L1L2 and LMLa, respectively, in the terminology of Hindmarsh, 2004.) The simulations for this paper use the depth-integrated solver, which gives a good balance between accuracy and efficiency for continental-scale simulations (Lipscomb et al., 2019).

CISM supports several basal sliding laws. For ISMIP6 projections we use a sliding law based on Schoof (2005), with a functional form suggested by Asay-Davis et al. (2016):

$$\boldsymbol{\tau_b} = \frac{C_p C_c N}{\left[C_p^m |\boldsymbol{u_b}| + (C_c N)^m\right]^{\frac{1}{m}}} |\boldsymbol{u_b}|^{\frac{1}{m}-1} \boldsymbol{u_b}, \tag{1}$$

where $\boldsymbol{\tau_b}$ is the basal shear stress, $\boldsymbol{u}$ is the basal ice velocity, N is the effective pressure, $m = 3$ is a power-law exponent, and C_p and C_c are empirical coefficients. In the ice sheet interior, where the ice is relatively slow-moving with large effective pressure, this law gives power-law behavior:

$$\boldsymbol{\tau}_b \approx C_p |\boldsymbol{u}|^{\frac{1}{m}-1} \boldsymbol{u}, \tag{2}$$

Where the ice is fast-moving with low effective pressure, we have Coulomb behavior:

$$\boldsymbol{\tau}_b \approx \frac{C_c}{N} \frac{\boldsymbol{u}}{|\boldsymbol{u}|}, \tag{3}$$

Since the power-law coefficient C_p is spatially variable and poorly constrained, we adjust $C_p(x, y)$ to nudge the ice thickness toward observed values, as described in section 3.1. The dimensionless Coulomb coefficient is set to $C_c = 0.5$, close to the value of 0.42 used by Pimentel et al. (2010). The effective pressure is set to the ice overburden pressure, $N = \rho_i g H$, where ρ_i is ice density and g is gravitational acceleration. We initially made N proportional to $(1 - H_f/H)$, where H_f is the flotation thickness, to represent the connection of subglacial water to the ocean (Leguy et al., 2014), but this choice led to excessive grounding-line retreat in some regions. Setting N to overburden pressure implies power-law behavior in nearly all of the ice sheet.

CISM also supports several calving laws, but none was found to give calving fronts in good agreement with observations for both large and small Antarctic ice shelves. Instead, we use a no-advance calving mask, removing all ice that flows beyond the observed calving front. The calving front can retreat where there is more surface and basal melting than advective inflow, but more often the calving front remains in place.

Many studies (e.g., Pattyn, 2006; Schoof, 2007) have emphasized the challenges of simulating ice dynamics in the transition zone between grounded and floating ice, especially when the grid resolution is ~ 1 km or coarser, as is the case for most simulations of whole ice sheets. Grounding line parameterizations (GLPs), which give a smooth transition in basal shear stress across the transition zone, have been shown to improve numerical accuracy in models with relatively coarse grids (e.g., Gladstone et al., 2010; Leguy et al., 2014; Seroussi et al., 2014). CISM has a GLP that was not used for the Greenland simulations in Lipscomb et al. (2019), but is used for Antarctic simulations and is described in Appendix A.

Finally, CISM supports several parameterizations of sub-ice-shelf melting. For Antarctic projections, the melt parameterizations are based on ISMIP6 protocols (see Sect. 2.2).

https://doi.org/10.5194/tc-2019-334
Preprint. Discussion started: 14 January 2020


The Cryosphere Discussions
Open Access
EGU

2.2 Protocols based on ISMIP6 for Antarctic projections

Protocols for the ISMIP6 Antarctic projections are described in detail by Nowicki et al. (in review) and Jourdain et al. (in review). Here, we give a brief summary, noting where the simulations in this paper differ from the protocols. The ISMIP6 projection experiments are run with standalone ice sheet models, forced by time-varying atmosphere and ocean fields derived from the output of CMIP5 and CMIP6 AOGCMs. (The simulations described here use only the ocean forcing.) The CMIP5 models were selected by a procedure described by Barthel et al. (2019) to sample the diversity in climate evolution around Antarctica. For CMIP6 models, there was not time for a formal selection, but output from selected models was processed as it became available. Each experiment runs for 86 years, from the start of 2015 to the end of 2100. Model initialization methods are left to the discretion of each group, and are detailed for specific models in Seroussi et al. (2019, in review). If the initialization date is before the start of the projections, a short historical run is needed to advance the ISM to the end of 2014.

For projections, ISMIP6 provides data sets of yearly atmosphere and ocean forcing on a standard 8-km grid. The ocean forcing consists of 3D fields of thermal forcing (i.e., the difference between the in situ ocean temperature and the in situ freezing temperature), obtained by a complex process described by Jourdain et al. (in review). It is not possible to use ocean temperature and salinity directly from AOGCMs, because current CMIP models do not simulate ocean properties in ice shelf cavities. Moreover, global ocean models are usually run at a resolution of $\sim 1^\circ$, too coarse to give an accurate mean state for ocean properties near Antarctic ice shelves. Instead, Jourdain et al. (in review) combined recent data sets (Locarnini et al., 2019; Zweng et al., 2019; Good et al., 2013; Treasure et al., 2017) to construct a 3D gridded climatology of ocean temperature and salinity. This climatology was interpolated to fill gaps and extrapolated into ice-shelf cavities. To obtain forcing fields for projections, temperature and salinity from the various AOGCM ocean models were extrapolated to cavities, and their anomalies were added to the observationally derived climatology. The result is a time-varying 3D product that can be vertically interpolated to give the thermal forcing at the base of a dynamic ice shelf at any time and location in the Antarctic domain.

To compute basal melt rates beneath ice shelves, ISMIP6 models can use a standard approach, an open approach, or both. The open approach is chosen independently by each modeling group; the only requirement is to use the ocean data provided by Jourdain et al. (in review). For the standard approach, basal melt rates beneath ice shelves are computed as a quadratic function of thermal forcing as suggested by Favier et al. (2019), with a thermal forcing correction suggested by Jourdain et al. (in review):

$$m(x,y) = \gamma_0 \times \left(\frac{\rho_w c_{pw}}{\rho_i L_f}\right)^2 \times (TF(x,y,z_{\text{draft}}) + \delta T_{\text{sector}}) \times |\langle TF\rangle_{\text{draft}\in\text{sector}} + \delta T_{\text{sector}}|\,, \tag{4}$$

where m is the melt rate, TF is the thermal forcing, γ_0 is an empirical coefficient, ρ_w and c_{pw} are the density and specific heat of seawater, and ρ_i and L_f are the density and latent heat of melting of ice. The brackets in $< TF >$ denote the average over a drainage basin or sector, and δT_{sector} is a thermal forcing correction with units of temperature, with one value per sector. The Antarctic Ice Sheet is divided into 16 sectors as shown in Fig. 1. Since this method uses sector-average thermal forcing, it is known as the *nonlocal* parameterization. For the simulations in this paper, the last term in Eq. 4 was modified to $\max(\langle TF\rangle_{\text{draft}\in\text{sector}} + \delta T_{\text{sector}}, 0)$ to avoid large and possibly spurious freezing rates in sectors with large negative values of δT.

https://doi.org/10.5194/tc-2019-334
Preprint. Discussion started: 14 January 2020

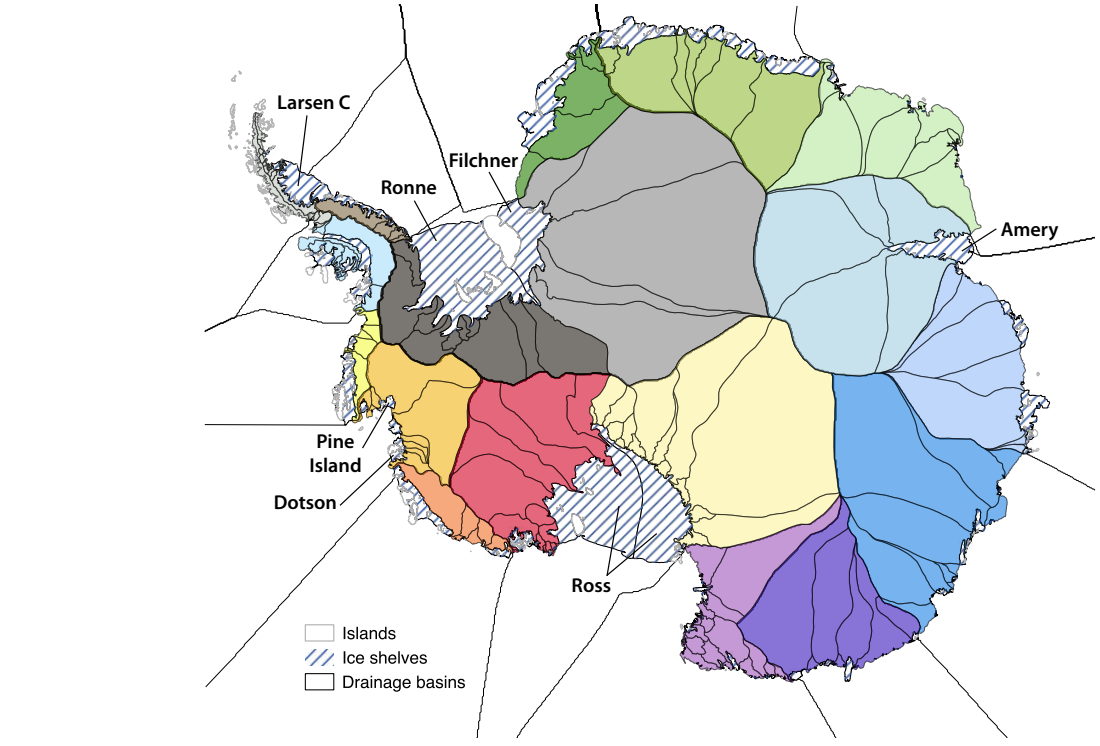

Figure 1. Individual drainage basins, ice shelves, and sectors (shading) defined by Mouginot et al. (2017) and Rignot et al. (2019). Reprinted with permission from Jourdain et al. (in review, their Fig. 2).

An alternative *local* parameterization is obtained by replacing $< TF >$ in the last term:

$$m(x,y) = \gamma_0 \times \left(\frac{\rho_w c_{pw}}{\rho_i L_f}\right)^2 \times \{\max\left[TF(x,y,z_{\text{draft}}) + \delta T_{\text{sector}}, 0\right]\}^2, \quad (5)$$

giving a quadratic dependence on the local thermal forcing. A third parameterization, which we call *nonlocal-slope* or simply *slope*, is obtained by multiplying Eq. 4 by $\sin(\theta)$, where θ is the local angle between the ice-shelf base and the horizontal. At the same time, γ_0 is increased by a factor of ~ 100, since $\sin(\theta)$ typically is $\sim 10^{-2}$. This scheme, suggested by Little et al. (2009) and Jenkins et al. (2018), generally gives larger melt rates near grounding lines and lower melt rates near the calving front, in agreement with observational estimates and ocean simulations (e.g., Rignot et al., 2013; Favier et al., 2019). Total melt over the ice sheet is the same, if γ_0 is tuned based on a total-melt criterion. CISM simulations in Seroussi et al. (in review) used the slope parameterization as an open approach.

Sub-ice-shelf thermal forcing and melt rates are uncertain, as is the functional relationship between thermal forcing and melt rates. For this reason, γ_0 and δT_{sector} are not well constrained. To calibrate Eqs. 4 and 5, Jourdain et al. (in review) used two methods. In the *MeanAnt* method, γ_0 is chosen so that the total Antarctic melt rate given by the parameterization matches the observational estimates of Depoorter et al. (2013) and Rignot et al. (2013), before applying basin-scale thermal forcing corrections. Then the δT_{sector} values are chosen to reproduce the estimated mean melt rate in each sector. The *PIGL* method

https://doi.org/10.5194/tc-2019-334
Preprint. Discussion started: 14 January 2020

is similar, except that the melt rate targets are given by observations in the Amundsen Sea sector near the grounding line of Pine Island Glacier (Rignot et al., 2013). The γ_0 values for the PIGL calibration are an order of magnitude larger than those obtained by the MeanAnt method, but the present-day average melt rates in each basin are similar with the two calibrations. (See Jourdain et al., in review for more details on these parameterizations and calibrations.)

The simulations in our paper differ from the ISMIP6 protocols in the treatment of δT_{sector}. Although we use calibrated values of γ_0, we tune δT_{sector} to better match the mean ice thickness near the grounding line, as described in Sect. 3.1. This procedure calibrates δT_{sector} to optimize melt rates near the grounding line where they matter most for ice extent, but also gives basin-average melt rates that differ from the observational estimates.

In summary, we have presented three basal melt parameterizations (local, nonlocal, and slope) and two calibration methods (MeanAnt and PIGL), giving six possible combinations (local-MeanAnt, nonlocal-PIGL, etc.). Values of γ_0 for each combination are shown in Table 1. These combinations form the basis for the ensemble of spin-up and forcing experiments described in Sects. 3 and 4.

Table 1. Calibrated γ_0 values for the three quadratic parameterizations and two calibration methods (in $\mathrm{m\,y^{-1}}$).

Parameterization	Calibration	γ_0
local	MeanAnt	1.11×10^4
nonlocal	MeanAnt	1.44×10^4
nonlocal-slope	MeanAnt	2.06×10^6
local	PIGL	4.95×10^4
nonlocal	PIGL	1.59×10^5
nonlocal-slope	PIGL	5.37×10^6

3 Model spin-up

3.1 Nudging procedure

When spinning up the model, we aim to to reach a stable state with minimal drift under modern forcing, while also simulating ice sheet properties that agree with observations. It is challenging to achieve both goals at once. Long spin-ups typically yield a steady-state ice sheet with large biases in thickness, velocity, and/or ice extent, while initialization methods that assimilate data to match present-day conditions often have a large initial transient. We compromised by using a hybrid method similar to that of Pollard and DeConto (2012), running a long spin-up while continually nudging the ice sheet toward the observed thickness.

Beneath grounded ice, we adjust $C_p(x, y)$, a poorly constrained, spatially varying friction coefficient in the basal sliding law (Eq. 1). This coefficient controls the power-law behavior (Eq. 2) in most of the ice sheet, with higher C_p giving greater friction and less sliding. Wherever grounded ice is present, C_p is initialized to $50{,}000\ \mathrm{Pa\,m^{-1/3}\,y^{-1}}$. During the spin-up, C_p is decreased where $H > H_{\text{obs}}$ and increased where $H < H_{\text{obs}}$, based on the idea that lower friction will accelerate the ice and

https://doi.org/10.5194/tc-2019-334
Preprint. Discussion started: 14 January 2020


The Cryosphere Discussions

lower the surface, while higher friction will slow the ice and raise the surface. The rate of change of C_p is given by

$$\frac{dC_p}{dt} = -\frac{C_p}{H_0}\left[\frac{(H - H_{\mathrm{obs}})}{\tau_c} + 2\frac{dH}{dt}\right], \tag{6}$$

where H_{obs} is an observational target, $H_0 = 100$ m is a thickness scale, and $\tau_c = 500$ y is a time scale for adjusting C_p. Eq. 6 is based on the equation for a critically damped harmonic oscillator, where the first term in brackets nudges H toward H_{obs}, and the second term damps the nudging to prevent overshoots. (The damping is not exactly critical, however, because dC_p/dt is not exactly proportional to d^2H/dt^2.) We hold C_p within a range between 10^2 and 10^5 Pa m$^{-1/3}$ y^{-1}, since smaller values can lead to numerical instability, and larger values do not significantly lower the sliding speed.

This method works well in keeping most of the grounded ice near the observed thickness. Also, since C_p is independent of the ice thermal state, we remove low-frequency oscillations associated with slow changes in basal temperature, resulting in a better-defined steady state. In forward runs, however, $C_p(x, y)$ is held fixed and cannot evolve in response to changes in basal temperature or hydrology. As a result, we can have unphysical basal velocities when the ice dynamics differs from the spun-up state.

Another nudging method is needed to initialize floating ice shelves, where $C_p = 0$. In CISM simulations for initMIP-Antarctica and ISMIP6 projections, (Seroussi et al., 2019, in review), basal melt rates were obtained by nudging. That is, an equation similar to Eq. 6 was used to nudge H toward H_{obs} by adjusting the melt rate $m(x, y)$ in each floating grid cell. In climate change experiments, the spun-up melt rates were added to prescribed melt rate anomalies in each basin. Although this method yields ice-shelf thicknesses and grounding-line locations that agree well with observations, it also overfits the observations, giving noisy melt rates that compensate for other errors without being tied to ocean temperatures. More complications arise when applying this spin-up method to the ISMIP6 projections, which prescribe thermal forcing anomalies instead of melt rate anomalies. In climate change experiments, a melt rate anomaly computed from the thermal forcing anomaly must be added to the spun-up melt rate, instead of computing the evolving melt rate directly from the evolving thermal forcing.

For the simulations described here (which were done too late to be included in Seroussi et al., in review), we take a different approach. During the spin-up, basal melt rates are computed directly from the thermal forcing, using the climatological data set and melt parameterizations described in Sect. 2.2. When we use the calibrated values of both γ_0 and $\delta T_{\mathrm{sector}}$, many grounding lines drift far from their observed locations. The drift can be reduced (but not eliminated) by continually adjusting $\delta T_{\mathrm{sector}}$ in each of 16 sectors (see Fig. 1), nudging toward an ice thickness target in a region near the grounding line. Here, "near the grounding line" is defined as having a value of a function f_{float} whose magnitude is less than a prescribed value:

$$|f_{\mathrm{float}}| = \left|-b - \frac{\rho_i}{\rho_w}H\right| < H_{\mathrm{thresh}}, \tag{7}$$

where b is the seafloor elevation (negative below sea level) and H_{thresh} is the prescribed threshold thickness. Where $f_{\mathrm{float}} > 0$, it is equal to the thickness of the ocean cavity, and where $f_{\mathrm{float}} < 0$, the ice is grounded. We set $H_{\mathrm{thresh}} = 400$ m, so that the target region includes most of the ice likely to switch between floating and grounded during a spin-up, without extending too far upstream.

https://doi.org/10.5194/tc-2019-334
Preprint. Discussion started: 14 January 2020

During the spin-up, δT in each sector is adjusted as follows:

$$\frac{d(\delta T)}{dt} = -\frac{1}{\tau_m m_T}\left[\frac{\bar{H} - \bar{H}_{\mathrm{obs}}}{\tau_m} + 2\frac{d\bar{H}}{dt}\right], \tag{8}$$

where $\bar{H}$ is the mean ice thickness over the target region, $\bar{H}_{\mathrm{obs}}$ is the observational target for this region, m_T is a scale for the rate of change of basal melt rate m with temperature T, and τ_m is a timescale for adjusting δT. As in Eq. 6, the first-derivative term damps oscillations. After some experimentation, we set $m_T = 10\ \mathrm{m\,y^{-1}\,K^{-1}}$ and $\tau_m = 10$ y. In most basins, this adjustment keeps $\bar{H}$ close to $\bar{H}_{\mathrm{obs}}$ with modest values of δT (~ 1 K or less). In some basins, $\bar{H} < \bar{H}_{\mathrm{obs}}$ no matter how much δT is lowered, and in these basins δT is capped at -2 K.

Given the calibrated thermal forcing, the melt rate m is computed for floating grid cells using one of the three parameterizations described in Sect. 2.2. A. In partly grounded cells, m is weighted by $1 - \phi_g$, where ϕ_g is the grounded fraction computed as described in Appendix A. In shallow cavities, following Asay-Davis et al. (2016), m is weighted by $\tanh(H_c/H_{c0})$, where H_c is the cavity thickness and $H_{c0} = 50$ m is an empirical depth scale.

Running CISM for several millennia while adjusting for C_p in each grounded grid cell and δT in each basin, the ice sheet approaches a steady state. We evaluate the spun-up state below.

3.2 Spun-up model state

We carried out six Antarctic spin-ups, each with a different pairing of the three basal melt parameterizations (local, nonlocal, and nonlocal-slope) and the two calibrations (MeanAnt and PIGL). For each spin-up, the ice sheet is initialized to present-day thickness using the BedMachineAntarctica data set (Morlighem et al., 2019) with analytic vertical temperature profiles. The surface mass balance and surface temperature are provided by a regional climate model, RACMO2.3 (van Wessem et al., 2018), and the geothermal heat flux is from Shapiro and Ritzwoller (2004). During each spin-up, the simulated ice thickness is nudged toward observations by adjusting $C_p(x, y)$ and $\delta T_{\mathrm{sector}}$ as described in Sect. 3.1. The spin-ups were run for 20,000 model years, allowing the ice sheet to come very close to steady state; at this time the total mass is changing by $< 1\ \mathrm{Gt\,y^{-1}}$.

Although γ_0 varies widely among the different spin-ups, the spun-up states are similar across parameterizations and calibrations, because of the freedom to adjust C_p and $\delta T_{\mathrm{sector}}$ independently for each run. The simulated thickness, velocity, and ice extent are broadly in agreement with observations, but with some persistent biases. Some biases can likely be attributed to errors in ocean thermal forcing (which is treated simply by the basin-scale melt parameterizations) and seafloor topography (e.g., an absence of pinning points, resulting in grounding-line retreat that can be compensated by spurious ocean cooling).

Fig. 2 shows the difference between the starting ice thickness (from observations) and final ice thickness for two spin-ups: nonlocal-MeanAnt and slope-PIGL. These two configurations are interesting to compare because, as shown in Sect. 4, the latter is much more sensitive to ocean warming. The spun-up states, however, are similar, with some shared biases. In both spin-ups, Thwaites Glacier is too thin and Pine Island Glacier is too thick; the Filchner-Ronne Ice Shelf is thin near the central grounding line but thick elsewhere; the Moscow University and Totten Glaciers in East Antarctica are thin; and there are similar thick/thin patterns for the Ross Ice Shelf. There are also a few differences; for example, the nonlocal-MeanAnt run has a thick bias near the Amery grounding line, and the slope-PIGL run has a large thin region on the Bellingshausen Sea side of the Ronne Shelf.

https://doi.org/10.5194/tc-2019-334
Preprint. Discussion started: 14 January 2020

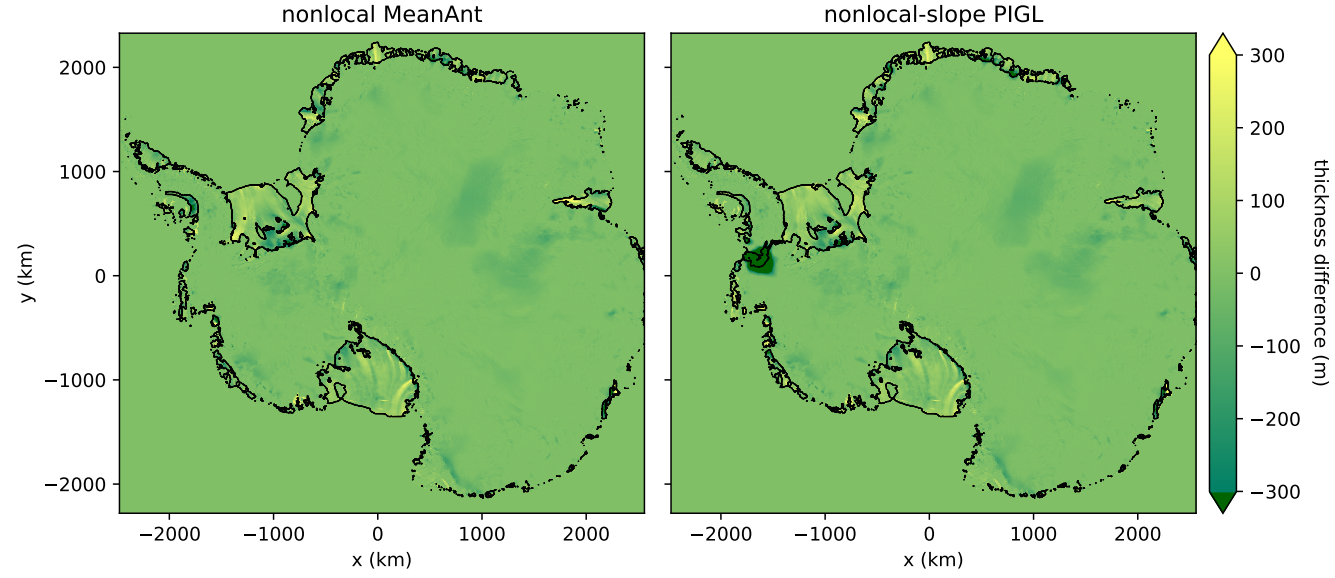

Figure 2. Difference in thickness (m) between the start and end of two 20 ky CISM spin-ups at 4-km resolution, for two combinations of melt parameterization and calibration: (left) nonlocal-MeanAnt and (right) nonlocal-slope-PIGL. Black contours show the extent of floating ice shelves at the end of the two spin-ups.

Fig. 3 compares ice surface speeds from the end of the nonlocal-MeanAnt spin-up to observed surface speeds (Rignot et al., 2011). Overall, the agreement with observations is very good for both grounded and floating ice, even though the model is nudged toward observed velocities only indirectly, via the thickness field. In general, we find that good agreement in thickness implies good agreement in velocity as well. (This is true, at least, when using BedMachineAntarctica thicknesses, which are obtained using the mass conservation method of Morlighem et al., 2011.) One place of disagreement is the Kamb Ice Stream on the Siple Coast, which is present in the model but absent in the observations, having stagnated in the 1800s but left a signature in the thickness field (Ng and Conway, 2004).

For the same spin-up, Fig. 4 shows ice surface speeds in the Amundsen Sea sector, including Pine Island and Thwaites Glaciers. The observations reveal a dual structure in the Thwaites velocity field, with a fast western core where the glacier flows into the Thwaites Ice Tongue, and slower speeds in the east where flow is impeded by an ice rise (cf. Fig. 1 in Rignot et al., 2014). The model, however, lacks a sharp division between east and west, and the Thwaites grounding line is retreated compared to observations, perhaps because the interaction with seafloor topography is not captured correctly. At the same time, the Pine Island grounding line is advanced compared to observations. The grounding lines of both glaciers have been retreating since at least the 1990s (Rignot et al., 2014), and the spin-up method is not well suited to initialize dynamic grounding lines in their observed locations.

Fig. 5 shows the values of the thermal forcing correction δT obtained for each sector at the end of the six spin-ups. In most sectors the corrections are modest (< 1 K in either direction). For the Wilkes and Aurora sectors in East Antarctica, however,

https://doi.org/10.5194/tc-2019-334
Preprint. Discussion started: 14 January 2020

The Cryosphere Discussions
Open Access
EGU

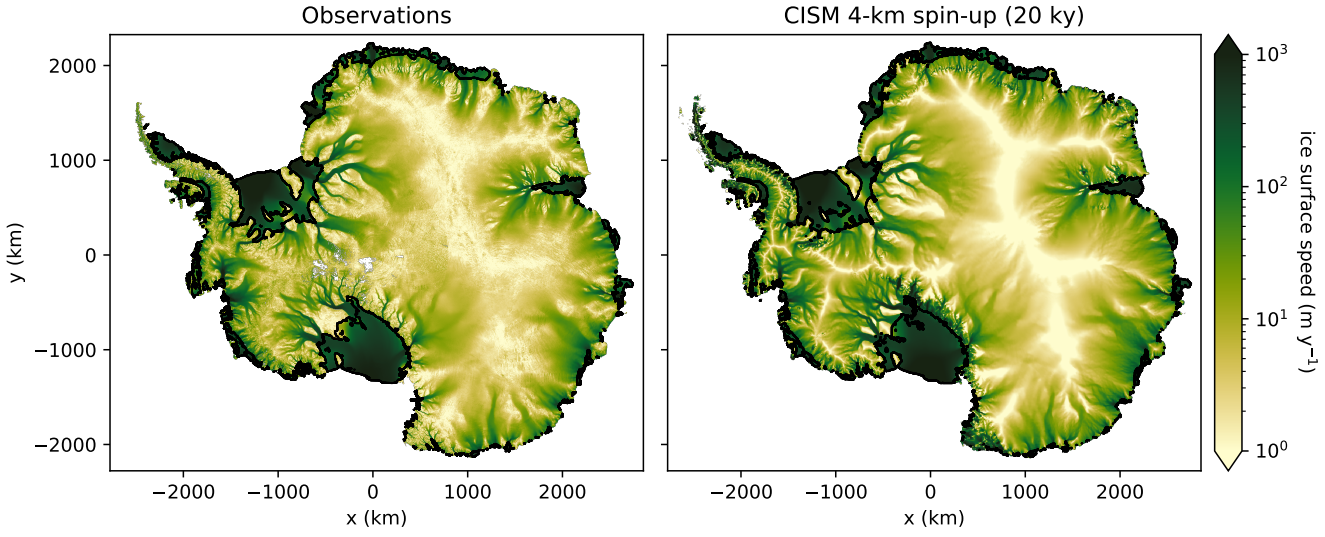

Figure 3. Antarctic ice surface speed ($\mathrm{m\,y^{-1}}$, log scale) from (left) observations (Rignot et al., 2011) and (right) the end of a 20 ky CISM spin-up at 4-km resolution using the nonlocal-MeanAnt melt parameterization and calibration. Black contours show the extent of floating ice shelves.

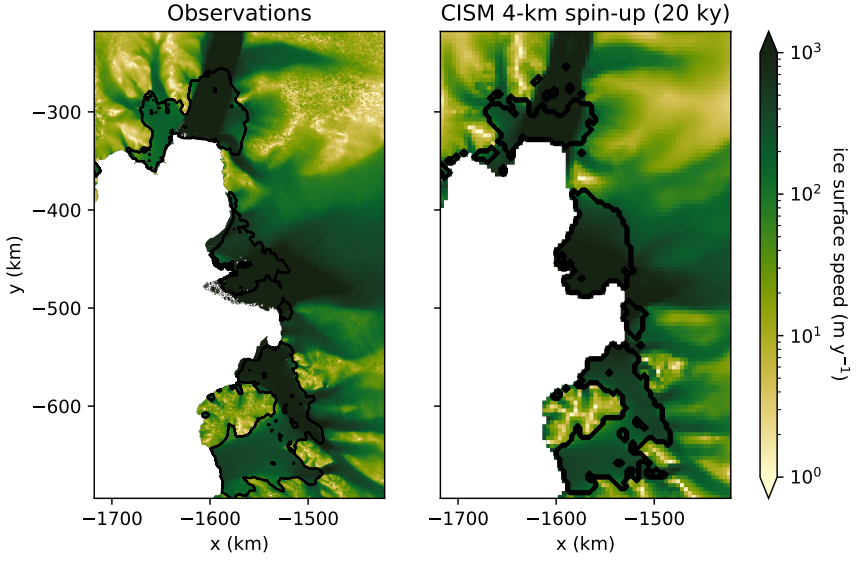

Figure 4. Ice surface speed ($\mathrm{m\,y^{-1}}$, log scale) for the Amundsen Sea sector from (left) observations and (right) the end of a 20 ky CISM spin-up at 4-km resolution using a nonlocal-MeanAnt melting combination. Black contours show the extent of floating ice shelves.

https://doi.org/10.5194/tc-2019-334
Preprint. Discussion started: 14 January 2020

δT is capped at -2 K, meaning that ice near the grounding line is biased thin, even when basal melting is reduced to zero. Also, δT is strongly negative for the Amundsen Sea sector, with values < -1 K for the PIGL calibration. This is the model's attempt to curtail the grounding-line retreat that occurs, especially for Thwaites Glacier, when γ_0 is large and δT is near 0. This means that melt rates might be underestimated in the spin-up, which could alter the sensitivity to future warming. A goal for future work is to reduce δT for these sectors through more realistic ocean forcing and/or seafloor topography.

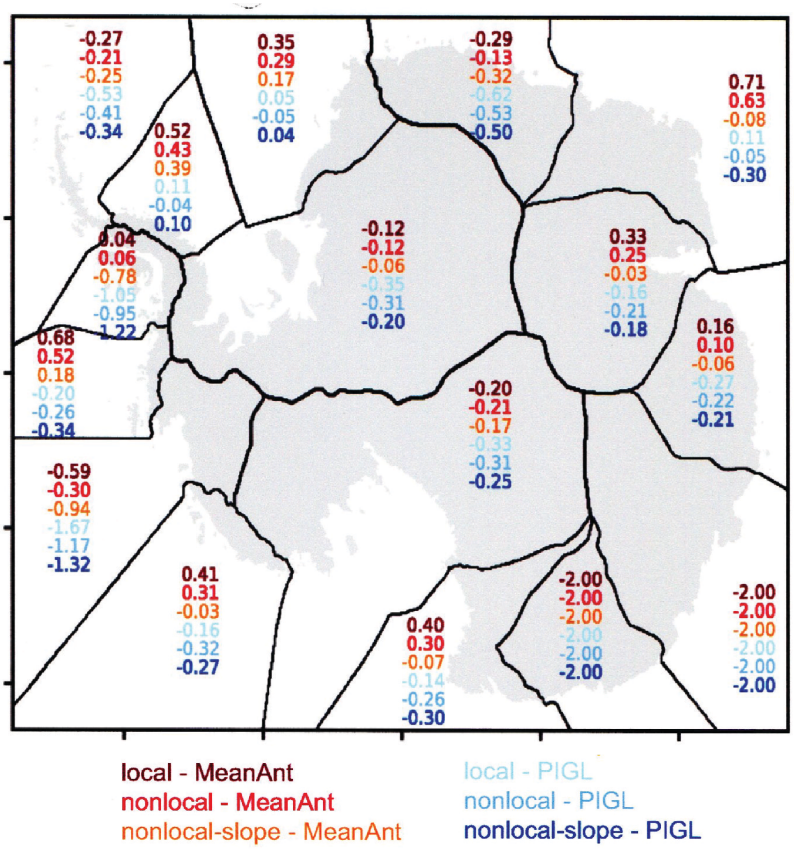

Figure 5. Values of the thermal forcing correction δT_{sector} in each of 16 sectors at the end of the CISM spin-ups, for six combinations of parameterization (local, nonlocal, and nonlocal-slope) and calibration (MeanAnt and PIGL).

Finally, we note that although the ice sheet mass budget is nearly in balance at the end of the spin-ups, total basal melt rates are 500–600 $\mathrm{Gt\,y^{-1}}$, about half the values estimated by Depoorter et al. (2013) and Rignot et al. (2013). Lower-than-observed

https://doi.org/10.5194/tc-2019-334
Preprint. Discussion started: 14 January 2020

melt rates are caused mainly by negative δT corrections, again suggesting that δT could be compensating for other model errors, such as too-fast flow in ice shelves that are too lightly buttressed.

4 Results of projection experiments

After finishing the six spin-ups described in Sect. 3, we ran 36 projection experiments with ocean thermal forcing from six CMIP AOGCMs. The four CMIP5 models are CCSM4, HadGEM2-ES (hereafter HadGEM2), MIROC-ESM-CHEM (hereafter MIROC), and NorESM1-M (hereafter NorESM1). These were among the top six CMIP5 models chosen by Barthel et al. (2019). CCSM4, MIROC, and NorESM1 were used for the ISMIP6 Tier 1 experiments, and we added HadGEM2 (a Tier 2 selection) to sample a model with relatively high ocean warming. The two CMIP6 models are CESM2 and UKESM, which are successors of CCSM4 and HadGEM2, respectively. All the AOGCMs ran high-end emissions scenarios: RCP8.5 for the CMIP5 models and SSP5-85 for the CMIP6 models. Each spun-up ice sheet state was run forward with ocean forcing from the six AOGCMs.

Fig. 6 shows the thermal forcing at ocean level 9 ($z = -510$ m) for these six models, averaged over 2081-2100. For each model, the forcing is relatively uniform across a given basin, with the Amundsen Sea the warmest of the three large WAIS basins. HadGEM2 and UKESM are both relatively warm in the Filchner-Ronne Basin, and somewhat less warm in the Ross Basin. NorESM1 is moderately warm for Filchner-Ronne and especially warm for Ross. CCSM4 and (to a lesser extent) CESM2 are moderately warm for Filchner-Ronne, and both are fairly cold for Ross, while MIROC is moderately warm for Ross and cold for Filchner-Ronne. These patterns are reflected in the ice loss discussed below.

We ran each projection experiment for 500 years starting in 1995, the nominal date of the spin-up. In the ISMIP6 protocols, the first 20 years (to the start of 2015) constitute a historical run and the remainder a projection run, but for our simulations the historical and projection periods were forced in the same way. From 1995–2100, we applied the yearly thermal forcing provided by ISMIP6. After 2100, we cycled repeatedly through the last 20 years of forcing, 2081–2100, to evaluate the committed SLR associated with a late-21$^{\text{st}}$ century climate. For comparison, we ran a subset of forcing experiments using a fixed climatology, computed as the mean of the 2081–2100 thermal forcing. Cycling through the yearly forcing drives greater mass loss (by $\sim 15\%$) than does the fixed climatology, suggesting that years with high thermal forcing have a disproportional influence on long-term mass loss, given the quadratic relationship between thermal forcing and melt rates.

Fig.7 shows time series of ocean-forced sea-level rise for the 36 projection experiments, with one panel per parameterization-calibration pair. Along with the CMIP-forced runs, each plot shows the SLR from a control run with no change in thermal forcing compared to the spin-up. SLR during the control runs is minimal, showing that the spin-ups have come close to steady state as desired.

Several patterns emerge. First, SLR starts slowly for all experiments, then accelerates near the end of the 21$^{\text{st}}$ century, suggesting that a threshold has been crossed based on some magnitude or duration of thermal forcing. After 2100, SLR is fairly linear and shows no sign of leveling off after 500 years. This is consistent with retreat driven by MISI in large reverse-

https://doi.org/10.5194/tc-2019-334
Preprint. Discussion started: 14 January 2020

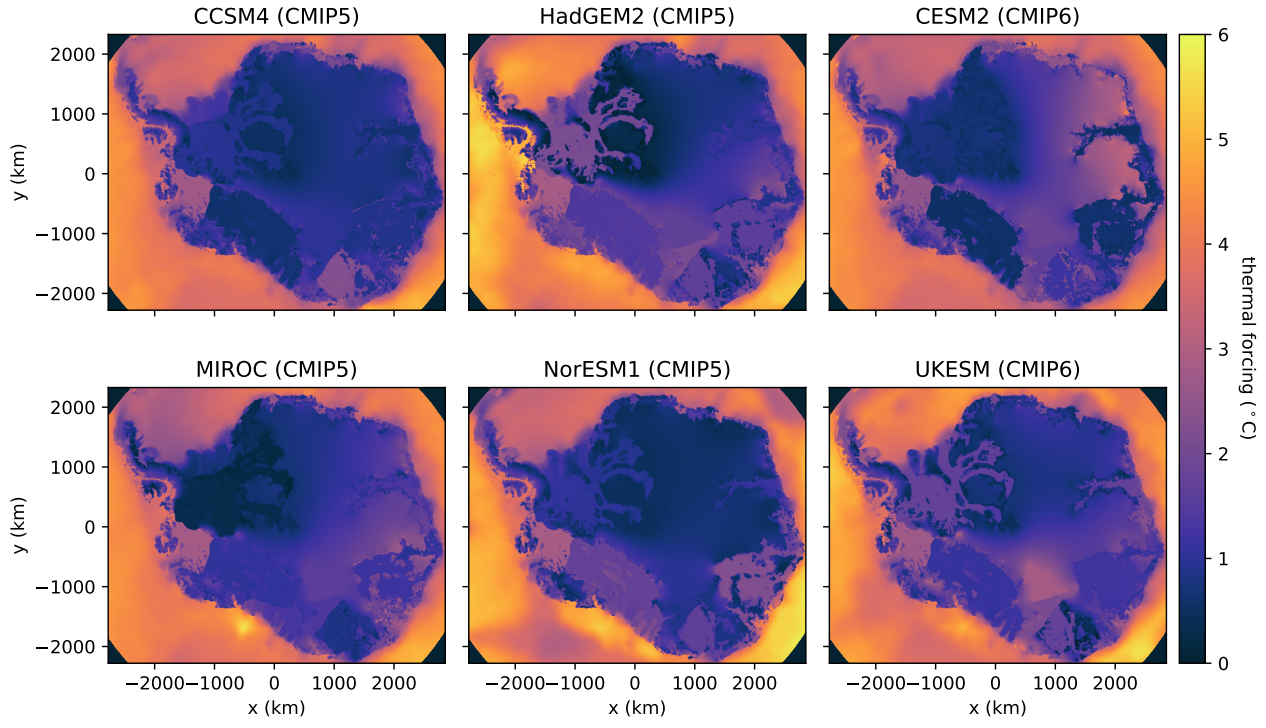

Figure 6. Ocean thermal forcing (°C) at $z = -510$ m, averaged over 2081–2100, for the four CMIP5 models and two CMIP6 models used in ocean-forced projection experiments.

sloping basins. Once the retreat is under way, it continues until reaching a stable seafloor configuration, up to several hundreds of km upstream.

Second, the ice sheet is more sensitive to some melt combinations than others. Sensitivity to local versus nonlocal parameterizations is similar. However, the nonlocal-slope parameterization yields more SLR than local and nonlocal, and the PIGL calibration gives more SLR than MeanAnt. The greater sensitivity for the slope scheme can be attributed to larger melt rates at steep slopes near grounding lines, where melting is most effective in driving ice retreat. The greater sensitivity of PIGL than MeanAnt results from the higher values of γ_0. During the spin-ups, PIGL runs acquire more negative values of δT than MeanAnt, to compensate for greater γ_0. Then, for a given thermal forcing anomaly during the forward runs, the rate of change of m (as given by Eqs. 4 and 5) is proportional to γ_0 and thus is larger for PIGL.

Third, the CMIP model rankings are consistent across melt schemes. HadGEM2 is the warmest model and drives the most SLR, followed by UKESM and then NorESM1. CCSM4 and CESM2 give similar rates of SLR, and MIROC yields the least. This ranking follows the magnitude of the thermal forcing in the various WAIS basins (Fig. 6). For a given model, the most sensitive melt scheme (slope-PIGL) yields up to 5 times as much SLR as the least sensitive schemes (local- and nonlocal-

https://doi.org/10.5194/tc-2019-334
Preprint. Discussion started: 14 January 2020

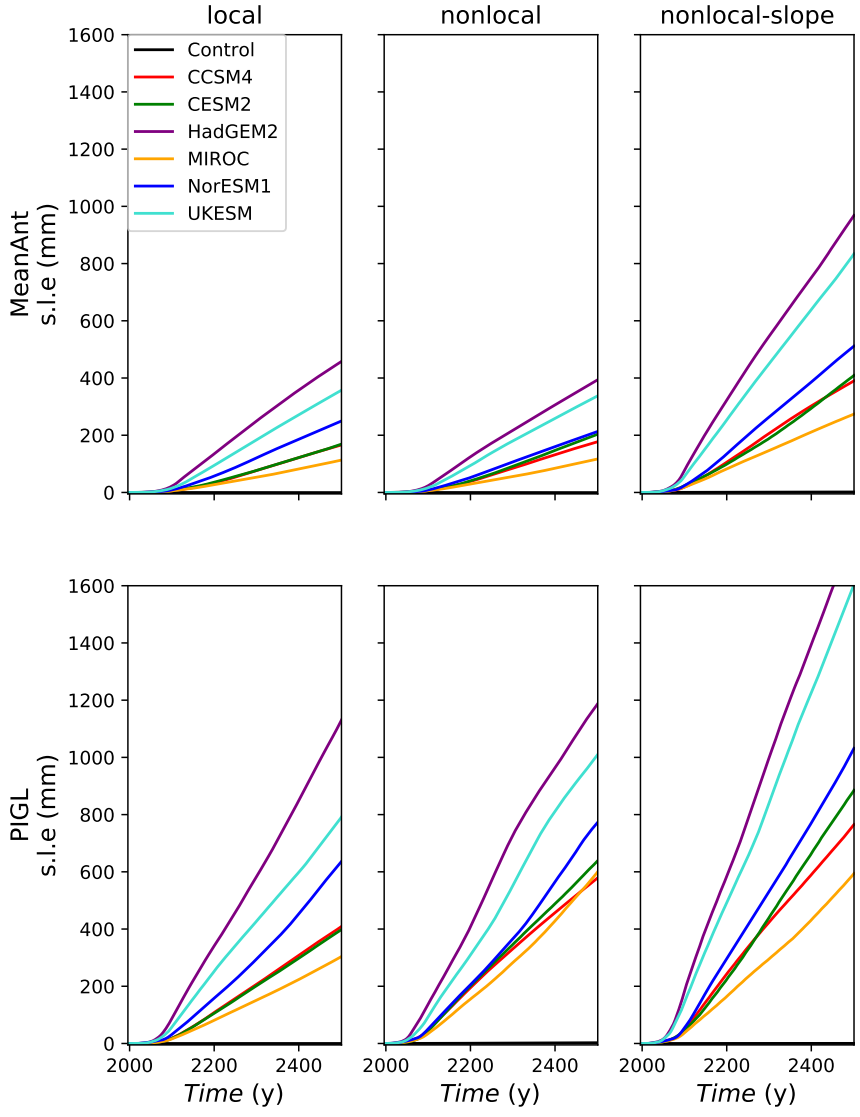

Figure 7. Sea-level rise from Antarctic ice sheet mass loss over 500 years for ocean-forced projection experiments. The three columns correspond to the three melt parameterizations, and the two rows to the two calibrations. Each panel shows the SLR response to ocean forcing from six AOGCMs, along with an unforced control run. The greatest SLR response (off the scale in the lower right plot) is 1790 mm, from the nonlocal-slope PIGL run with HadGEM2 forcing.

https://doi.org/10.5194/tc-2019-334
Preprint. Discussion started: 14 January 2020

MeanAnt), and the warmest model (HadGEM2) drives 2 to 4 times as much SLR as the coolest (MIROC). Thus, the total SLR over 500 years varies by a factor of about 20, from ~ 10 cm to almost 2 m.

Fig. 8 shows spatial plots of thickness changes from a subset of projection runs. These plots are similar to Fig. 2, except that the field shown is not the difference in ice thickness, but rather the difference in thickness above flotation—in other words, the part of the ice column that contributes to SLR. The figure shows results from projection runs for three AOGCMs (HadGEM2, NorESM1, and CESM2) and for nonlocal-MeanAnt and nonlocal-slope-PIGL, the least and most sensitive melt combinations.

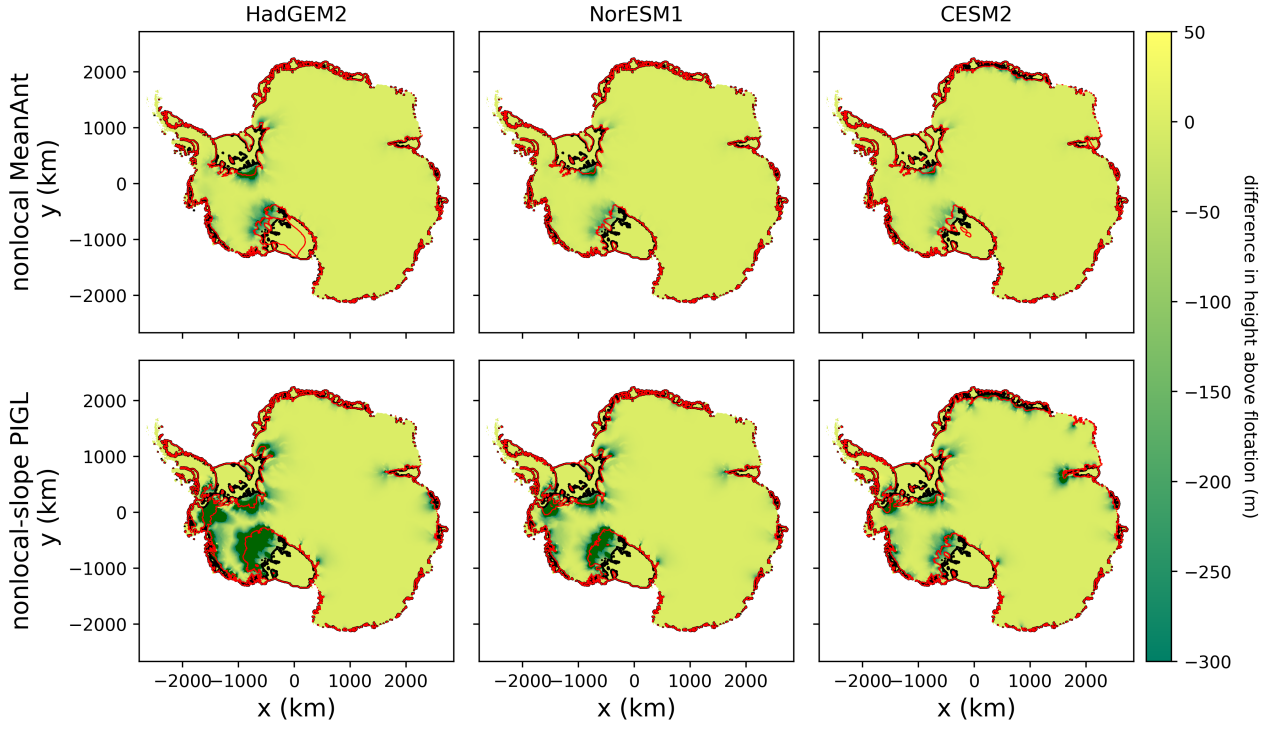

Figure 8. Change in ice thickness above flotation during ocean-forced 500-year projection experiments. The top and bottom rows show results from the nonlocal-MeanAnt and slope-PIGL melt combinations, respectively. The three columns show results with ocean forcing from HadGEM2, NorESM1, and CESM2.

Most of the SLR contribution comes from the large WAIS basins on reverse-sloping beds: Amundsen Sea, Filchner-Ronne, and Ross. In most cases the Amundsen Sea contribution is smaller than the Filcher-Ronne and/or Ross contributions, which is unexpected given that the Amundsen Sea sector dominates current WAIS retreat. It is possible that the melt parameterizations underestimate the delivery of heat to Amundsen Sea grounding lines, in part because of the large negative δT corrections discussed in Sect. 3.2. Conversely, the extrapolation procedure and melt parameterizations might overestimate heat delivery to the Filchner-Ronne and Ross cavities, which currently have little basal melting. Although some ocean models with CMIP3 atmospheric forcing have projected Weddell Sea warming (e.g., Hellmer et al., 2012; Timmermann and Hellmer, 2013), it is not clear that these large shelves will readily transition from cold, low-melt regimes to warm, high-melt regimes (Naughten

https://doi.org/10.5194/tc-2019-334
Preprint. Discussion started: 14 January 2020

et al., 2018). Compared to the WAIS, there is a relatively small SLR contribution from East Antarctica, apart from the Amery Glacier region in the slope-PIGL runs.

.

5 Conclusions

Using the Community Ice Sheet Model, we ran an ensemble of ice sheet simulations based on the protocols for the ISMIP6 Antarctic projections (Nowicki et al., in review). We carried out six spin-ups to sample combinations of three basal melt parameterizations (local, nonlocal, and nonlocal-slope), and two calibrations (MeanAnt and PIGL, as described by Jourdain et al., in review). In each spin-up, the model was nudged toward present-day ice thickness by adjusting friction parameters in a basal sliding law and adjusting basin-scale thermal forcing corrections in the melt parameterizations. The resulting spun-up states are similar across melt schemes, with minimal drift. The ice thickness, velocity, and shelf extent are generally in good agreement with observations, but there are persistent errors in grounding line locations, such as a Thwaites grounding line that is too far retreated.

From the spun-up states, we ran each ensemble member forward for 500 years, applying ISMIP6 ocean thermal forcing for 1995–2100 and cycling repeatedly through the 2081–2100 forcing for the rest of the simulation. Using forcing from four CMIP5 models and two CMIP6 models, we ran 36 projection experiments. For each simulation we analyzed the ice mass loss and associated sea level rise. In all cases, the Antarctic Ice Sheet loses mass, with total losses ranging from about 10 cm to nearly 2 m SLE. Mass loss begins slowly, accelerates in the late 21$^{\text{st}}$ century, and continues steadily for the next several centuries without leveling off. The thinning of grounded ice (i.e., ice that contributes to SLR) is concentrated in the Amundsen, Filchner-Ronne, and Ross Basins of WAIS, all of which have reverse-sloping beds and are vulnerable to marine ice sheet instability. East Antarctica loses relatively little grounded ice.

These simulations are consistent with recent studies (e.g., Cornford et al., 2015; Pollard and DeConto, 2016; Larour et al., 2019) showing potential WAIS collapse, driven by ocean warming in regions with reverse-sloping beds. The novelty of this study lies in the application of the ISMIP6 Antarctic forcing protocols (with melt rates derived from the new thermal forcing data of Jourdain et al., in review) to an ensemble of multi-century simulations. The results suggest that, by the end of this century (assuming high-end emissions scenarios), sub-ice-shelf melt rates could be large enough, if sustained, to drive the steady and possibly irreversible retreat of much of WAIS.

Ice loss is greater with the slope parameterization than with the local and nonlocal parameterizations, and greater with the PIGL calibration (which has higher values of the melt parameter γ_0) than with MeanAnt. Mass loss varies by a factor of about 5 between the most sensitive melt scheme (slope-PIGL) and the least sensitive (local- and nonlocal-MeanAnt), even when the ocean forcing comes from the same AOGCM. All the melt schemes leave out important physics, and it is not known whether one parameterization or calibration is more accurate than the others. Similarly, ice loss varies by a factor of 2 to 4 between the warmest AOGCM (HadGEM2) and the coolest (MIROC), even when using the same melt scheme. Thus, while suggesting that much of WAIS is vulnerable to projected ocean warming, these results do not place firm bounds on the rate of future SLR.

https://doi.org/10.5194/tc-2019-334
Preprint. Discussion started: 14 January 2020

Ice sheet retreat in these simulations is modest for the next several decades. It is not clear to what extent this inertia is real, rather than an artifact of the spin-up procedure. The model starts close to steady state, nominally in 1995, with no attempt to assimilate retreat that was already under way (e.g., Rignot et al., 2019). Several ISMs in the ISMIP6 Antarctic ensemble (Seroussi et al., in review) use similar spin-up methods that could underestimate near-term ice loss. (Other models use data assimilation techniques that are better equipped to capture ongoing trends.) Given this inertia, Antarctic projections ending in 2100 (largely for practical reasons, since CMIP forcing data often is unavailable after 2100) do not give a full picture of sea-level commitment from ice sheet retreat. It is possible that ocean warming during this century could result in a commitment of several meters from WAIS, but with most of the SLR taking place in future centuries.

To these conclusions, we add several caveats. First, the inversion procedure gives large and possibly spurious negative temperature corrections for the Amundsen Sea basin, perhaps compensating for the absence of pinning points (e.g., for Thwaites Glacier). For this reason, Amundsen Sea retreat—which already is proceeding vigorously—might be underestimated.

Second, the ocean data extrapolation transfers AOGCM heat anomalies from the open ocean to the distant grounding lines of the Filchner-Ronne and Ross shelves, where present-day melting is minimal. To the extent that the simple melt schemes deliver too much heat to grounding lines, the Filchner-Ronne and Ross retreat would be overestimated.

More generally, these simulations leave out many physical processes and feedbacks. Changes in atmospheric forcing are omitted by design, to simplify the analysis; increased snowfall in the ISMIP6 multi-model ensemble can mitigate the mass loss from ocean forcing (Seroussi et al., in review). In terms of ice sheet physics, these simulations do not include hydrofracture or calving-front retreat, and thus are missing positive feedbacks associated with reduced buttressing of grounded ice by ice shelves (Sun et al., in review). Solid-Earth and sea-level feedbacks are missing; these have been found to delay (but not prevent) long-term ice retreat in the Thwaites basin (Larour et al., 2019). At 4-km grid resolution, processes such as grounding-line retreat may be under-resolved. Moreover, the depth-based melt parameterizations ignore important process such as eddy heat transfer onto the continental shelf (Stewart and Thompson, 2015) and topographic steering. Without these processes, thermal forcing in cavities could be missing critical spatial structure. Finally, there is no interaction between the ice sheet and the cavity circulation or open ocean, so that the freshwater fluxes from increased melting are unable to modify the thermal forcing.

These uncertainties suggest several lines of research to further improve ice-sheet and sea-level projections:

- Running similar long-term simulations with multiple ice sheet models, to quantify structural ISM uncertainties.
- Extending more CMIP AOGCM simulations beyond 2100, to generate forcing for multi-century ice sheet simulations.
- Forcing ISMs with a greater variety of scenarios, including overshoot scenarios to study whether WAIS retreat, once begun, could be stopped or reversed.
- Adding more realistic physical processes and feedbacks, such as hydrofracture and solid-Earth/sea-level effects. Some ISMs already simulate these processes, and a subset of the ISMIP6 Antartic projections included hydrofracture.
- Continuing to develop comprehensive data sets of sub-ice-shelf melt rates and Southern Ocean temperature and salinity, to better force models and validate parameterizations.

https://doi.org/10.5194/tc-2019-334
Preprint. Discussion started: 14 January 2020

- Running regional, high-resolution simulations of the coupled ice shelf–ocean system. Such simulations are planned for the Weddell Sea and Amundsen Sea sectors during the second phase of the Marine Ice Sheet–Ocean Model Intercomparison Project (MISOMIP2).
- Developing simpler models of ice–ocean cavities and sub-shelf melting, which can emulate the results of high-resolution models but are efficient enough to run for long timescales in global models.
- Incorporating interactive ice sheet–ocean coupling in the next generation of Earth system models.

Many of these efforts are already under way and could contribute to future intercomparison projects, including the anticipated ISMIP7.

Appendix A: CISM's grounding-line parameterization

Grounded ice sheets and floating ice shelves are linked by a transition zone where flow dominated by vertical shear transitions to flow dominated by extensional stress. Without special numerical treatment, very fine grid resolution (~ 100 m) may be needed to accurately resolve the transition zone. Coarser resolution ($\sim 1-2$ km) may be sufficient, however, if a grounding-line parameterization (GLP) is used to treat basal friction (Gladstone et al., 2010; Leguy et al., 2014; Seroussi et al., 2014). Near the grounding line, GLPs typically compute the basal friction as an area-weighted average of the (possibly large) friction beneath grounded ice and zero friction beneath floating ice.

The GLP in CISM's Glissade dynamical core is similar to the PA_GB1 scheme of Gladstone et al. (2010), extended to two dimensions. Ice thickness H and bed elevation b (with $b < 0$ below sea level) are located at cell centers. Ice is deemed to be floating if it satisfies a flotation condition:

$$\rho_i H < (-\rho_w b), \tag{A1}$$

where ρ_i is the density of ice and ρ_w is the density of seawater. Based on this condition, we define a flotation function which depends linearly on H and b:

$$f_{\mathrm{float}} = -\rho_w b - \rho_i H, \tag{A2}$$

which gives $f_{\mathrm{float}} = 0$ at the grounding line, $f_{\mathrm{float}} < 0$ for grounded ice, and $f_{\mathrm{float}} > 0$ for floating ice. When positive, f_{float} is equal to the depth of the ocean cavity between the ice-shelf base and the seafloor.

Given f_{float} at cell centers, Glissade uses bilinear interpolation to compute a grounded ice fraction ϕ_g, which is located at vertices and lies in the range [0,1]. The value of ϕ_g at a vertex is set to the grounded area in a rectangular box that bounds the vertex. The corners of this box are the four neighboring cell centers, each with a value of f_{float} that determines whether the ice at that point is floating. The number of floating cells n_{float} surrounding a vertex can be 0, 1, 2, 3 or 4. For $n_{\mathrm{float}} = 0$ the ice at the vertex is fully grounded with $\phi_g = 1$. Likewise, $n_{\mathrm{float}} = 4$ implies $\phi_g = 0$. In the intermediate cases $n_{\mathrm{float}} = 1$, 2 or 3, the grounding line passes through the bounding box, giving $0 < \phi_g < 1$. There are three configurations to consider:

https://doi.org/10.5194/tc-2019-334
Preprint. Discussion started: 14 January 2020

1. One cell is grounded and three are floating (or vice versa). In this case the grounding line passes through two adjacent edges of the box.

2. Two adjacent cells (which share an edge) are grounded, and the other two cells are floating. In this case the grounding line passes through two opposite edges of the box.

3. Two cells at opposite corners of the box are grounded, and the other two are floating. In this case the grounding line passes through all four edges of the box, with one segment passing through two adjacent edges and another segment passing through the other two adjacent edges.

We compute ϕ_g as the fraction of the bounding box for which $f_{\text{float}} < 0$. We write f_{float} as a bilinear function of x and y:

$$f_{\text{float}}(x,y) = a + bx + cy + dxy, \tag{A3}$$

where x and y are scaled to vary between 0 and 1. With the southwest corner at $(0,0)$ and the northeast corner at $(1,1)$, the coefficients are

$$\begin{aligned} a &= f^{SW}, \\ b &= f^{SE} - f^{SW}, \\ c &= f^{NW} - f^{SW}, \\ d &= f^{NE} + f^{SW} - f^{NW} - f^{SE}, \end{aligned} \tag{A4}$$

where we have dropped the subscript "float".

To give an example, suppose the southwest cell is grounded and the other three are floating. The grounding line then passes through the west and south edges of the bounding box. Along the south edge we have $y = 0$ and therefore $f = a + bx$. Setting $f = 1$, we find that the grounding line intersects the south edge at $x_0 = (1-a)/b$. The equation for the grounding line is $a+bx+cy+dxy = 1$, from which it follows that $y = (1-a-bx)/(c+dx)$ along the grounding line. The area of the grounded southwest corner of the cell can then be obtained analytically (e.g., with the aid of an online integral calculator):

$$\phi_g = \int_0^{x_0} y(x)dx = \frac{(bc-ad+d)\ln\left(1+\frac{d(1-a)}{bc}\right) - (1-a)d}{d^2}. \tag{A5}$$

When $d = 0$, the integral reduces to

$$\lambda_g = \frac{(a-1)^2}{2bc}. \tag{A6}$$

The integrals for other configurations of floating and grounded cells can also be found analytically.

The grounded fraction ϕ_g at each vertex enters the ice dynamics via the basal friction coefficient β, defined as the ratio of basal shear stress to velocity:

$$\tau_{\mathbf{b}} = \beta \mathbf{u} \tag{A7}$$

https://doi.org/10.5194/tc-2019-334
Preprint. Discussion started: 14 January 2020

After β is found at each vertex using the chosen sliding law, it is multiplied by ϕ_g, and the result is used in the basal friction terms of the solution matrix. Since ϕ_g varies smoothly and linearly with H and b, the basal friction varies smoothly as the grounding line migrates, improving the numerical behavior of the velocity solution.

This is the procedure CISM uses to compute a grounded fraction ϕ_g at vertices. A similar algorithm is used to compute ϕ_g at cell centers for the purpose of weighting basal melting in cells that are partly grounded, as described in Section 3.1.

Code availability. CISM is an open-source code developed on the Earth System Community Model Portal (ESCOMP) git repository at *https://github.com/ESCOMP/CISM*. The version used for these runs is tagged as *ISMIP6_Antarctica_TC2019*.

Data availability. The model configuration and output files for the spin-ups described in Sect. 3 and the projection experiments in Sect. 4 will be archived on the NCAR Climate Data Gateway at *https://www.earthsystemgrid.org/*.

Author contributions. WHL conceived the study, designed the spin-up procedure, and developed CISM as needed to run the ISMIP6 experiments. WHL and GRL staged, ran, and analyzed the simulations. NCJ and XAD created the thermal forcing data sets and calibrated the melt parameterizations. HS coordinated Antarctic projections for ISMIP6, and SN led the overall ISMIP6 project. WHL and GRL wrote the paper with contributions from all authors.

Competing interests. William Lipscomb, Sophie Nowicki, and Hélène Seroussi are editors of the ISMIP6 special issue of *The Cryosphere*. The authors declare no other competing interests.

Acknowledgements. We thank the Climate and Cryosphere (CliC) project, which provided support for ISMIP6 through sponsoring of workshops, hosting the ISMIP6 website and wiki, and promoting ISMIP6. We acknowledge the World Climate Research Programme, which, through its Working Group on Coupled Modelling, coordinated and promoted CMIP5 and CMIP6. We thank the climate modeling groups for producing and making available their model output, the Earth System Grid Federation (ESGF) for archiving the CMIP data and providing access, the University at Buffalo for ISMIP6 data distribution and upload, and the multiple funding agencies who support CMIP5 and CMIP6 and ESGF. We thank the ISMIP6 steering committee, the ISMIP6 model selection group and ISMIP6 dataset preparation group for their continuous engagement in defining ISMIP6. We thank Mathieu Morlighem for early access to the BedMachineAntarctica data set. We are grateful to Bill Sacks and Kate Thayer-Calder for software engineering support, and to the entire ISMIP6 community for stimulating discussions.

This material is based upon work supported by the National Center for Atmospheric Research, which is a major facility sponsored by the National Science Foundation under Cooperative Agreement No. 1852977. Computing and data storage resources, including the Cheyenne supercomputer (doi:10.5065/D6RX99HX), were provided by the Computational and Information Systems Laboratory (CISL) at

https://doi.org/10.5194/tc-2019-334
Preprint. Discussion started: 14 January 2020

NCAR. NJ is funded by the French National Research Agency (ANR) through the TROIS-AS project (ANR-15-CE01-0005-01) and by the European Commission through the TiPACCs project (grant 820575, call H2020-LC-CLA-2018-2). Support for XAD was provided through the Scientific Discovery through Advanced Computing (SciDAC) program funded by the US Department of Energy (DOE), Office of Science, Advanced Scientific Computing Research and Biological and Environmental Research Programs. HS and SN were supported by grants from the NASA Cryospheric Science and Modeling, Analysis and Prediction Programs, and the NASA Sea Level Change Team.

This is ISMIP6 contribution No X.

https://doi.org/10.5194/tc-2019-334
Preprint. Discussion started: 14 January 2020

References

Asay-Davis, X. S., Cornford, S. L., Durand, G., Galton-Fenzi, B. K., Gladstone, R. M., Gudmundsson, G. H., Hattermann, T., Holland, D. M., Holland, D., Holland, P. R., Martin, D. F., Mathiot, P., Pattyn, F., and Seroussi, H.: Experimental design for three interrelated marine ice sheet and ocean model intercomparison projects: MISMIP v. 3 (MISMIP+), ISOMIP v. 2 (ISOMIP+) and MISOMIP v. 1 (MISOMIP1), Geosci. Model Dev., 9, 2471–2497, https://doi.org/10.5194/gmdd-9-2471-2016, 2016.

Barthel, A., Agosta, C., Little, C. M., Hatterman, T., Jourdain, N. C., Goelzer, H., Nowicki, S., Seroussi, H., Straneo, F., and Bracegirdle, T. J.: CMIP5 model selection for ISMIP6 ice sheet model forcing: Greenland and Antarctica, The Cryosphere Discussions, 2019, 1–34, https://doi.org/10.5194/tc-2019-191, 2019.

Blatter, H.: Velocity and stress fields in grounded glaciers - a simple algorithm for including deviatoric stress gradients, J. Glaciol., 41, 333–344, 1995.

Cornford, S. L., Martin, D. F., Payne, A. J., Ng, E. G., Le Brocq, A. M., Gladstone, R. M., Edwards, T. L., Shannon, S. R., Agosta, C., van den Broeke, M. R., et al.: Century-scale simulations of the response of the West Antarctic Ice Sheet to a warming climate, The Cryosphere, 9, 2015.

Cornford, S. L., Seroussi, H., Asay-Davis, X., Gudmundsson, G. H., Arthern, R., Borstad, C., Christmann, J., dos Santos, T. D., Feldmann, J., Goldberg, D., Hoffman, M., Humbert, A., Kleiner, T., Leguy, G., Lipscomb, W. H., Merino, N., Morlighem, M., Pollard, D., Rückamp, M., Williams, C. R., and Yu, H.: Results of the third Marine Ice Sheet Model Intercomparison Project (MISMIP+), The Cryosphere, in review.

Danabasoglu, G. et al.: The Community Earth System Model version 2 (CESM2), J. Adv. Model. Earth Syst., in review.

De Rydt, J. and Gudmundsson, G. H.: Coupled ice shelf-ocean modeling and complex grounding line retreat from a seabed ridge, J. Geophys. Res., 121, 865–880, 2016.

Depoorter, M. A., Bamber, J. L., Griggs, J. A., Lenaerts, J. T. M., Ligtenberg, S. R. M., van den Broeke, M. R., and Moholdt, G.: Calving fluxes and basal melt rates of Antarctic ice shelves, Nature, 502, 89–92, 2013.

Dutton, A., Carlson, A. E., Long, A. J., Milne, G. A., Clark, P. U., DeConto, R., Horton, B. P., Rahmstorf, S., and Raymo, M. E.: Sea-level rise due to polar ice-sheet mass loss during past warm periods, Science, 349, aaa4019, https://doi.org/10.1126/science.aaa4019, 2015.

Edwards, T. L., Brandon, M. A., Durand, G., Edwards, N. R., Golledge, N. R., Holden, P. B., Nias, I. J., Payne, A. J., Ritz, C., and Wernecke, A.: Revisiting Antarctic ice loss due to marine ice-cliff instability, Nature, 566, 58, 2019.

Eyring, V., Bony, S., Meehl, G. A., Senior, C. A., Stevens, B., Stouffer, R. J., and Taylor, K. E.: Overview of the Coupled Model Intercomparison Project Phase 6 (CMIP6) experimental design and organization, Geoscientific Model Development, 9, 1937–1958, 2016.

Favier, L., Durand, G., Cornford, S. L., Gudmundsson, G. H., Gagliardini, O., Gillet-Chaulet, F., Zwinger, T., Payne, A. J., and Le Brocq, A. M.: Retreat of Pine Island Glacier controlled by marine ice-sheet instability, Nature Climate Change, 4, 117–121, 2014.

Favier, L., Jourdain, N. C., Jenkins, A., Merino, N., Durand, G., Gagliardini, O., Gillet-Chaulet, F., and Mathiot, P.: Assessment of sub-shelf melting parameterisations using the ocean-ice sheet coupled model NEMO (v3. 6)-Elmer/Ice (v8. 3), Geoscientific Model Development, 2019.

Gladstone, R. M., Payne, A. J., and Cornford, S. L.: Parameterising the grounding line in flow-line ice sheet models, The Cryosphere, 4, 605–619, 2010.

Goelzer, H., Nowicki, S., Edwards, T., Beckley, M., Abe-Ouchi, A., Aschwanden, A., Calov, R., Gagliardini, O., Gillet-Chaulet, F., Golledge, N. R., Gregory, J., Greve, R., Humbert, A., Huybrechts, P., Kennedy, J. H., Larour, E., Lipscomb, W. H., Le clec'h, S., Lee, V., Morlighem,

https://doi.org/10.5194/tc-2019-334
Preprint. Discussion started: 14 January 2020

M., Pattyn, F., Payne, A. J., Rodehacke, C., Rückamp, M., Saito, F., Schlegel, N., Seroussi, H., Shepherd, A., Sun, S., van de Wal, R., and Ziemen, F. A.: Design and results of the ice sheet model initialisation experiments initMIP-Greenland: an ISMIP6 intercomparison, The Cryosphere, 12, 1433–1460, https://doi.org/10.5194/tc-12-1433-2018, 2018.

Goelzer, H., Nowicki, S., Payne, A., Larour, E., Seroussi, H., Lipscomb, W. H., Gregory, J., Abe-Ouchi, A., Shepherd, A., Simon, E., Agosta, C., Alexander, P., Aschwanden, A., Barthel, A., Calov, R., Chambers, C., Choi, Y., Cuzzone, J., Dumas, C., Edwards, T., Felikson, D., Fettweis, X., Golledge, N. R., Greve, R., Humbert, A., Huybrechts, P., clec'h, S. L., Lee, V., Leguy, G., Little, C., Lowry, D. P., Morlighem, M., Nias, I., Quiquet, A., Rückamp, M., Schlegel, N.-J., Slater, D., Smith, R., Straneo, F., Tarasov, L., van de Wal, R., , and van den Broeke, M.: The future sea-level contribution of the Greenland ice sheet: a multi-model ensemble study of ISMIP6, The Cryosphere, in review.

Goldberg, D. N.: A variationally derived, depth-integrated approximation to a higher-order glaciological flow model, J. Glaciol., 57, 157–170, https://doi.org/10.3189/002214311795306763, 2011.

Gomez, N., Mitrovica, J. X., Huybers, P., and Clark, P. U.: Sea level as a stabilizing factor for marine-ice-sheet grounding lines, Nature Geo., 3, 850–853, https://doi.org/10.1038/ngeo1012, 2010.

Good, S. A., Martin, M. J., and Rayner, N. A.: EN4: Quality controlled ocean temperature and salinity profiles and monthly objective analyses with uncertainty estimates, J. Geophys. Res. Oceans, 118, 6704–6716, 2013.

Hellmer, H. H., Kauker, F., Timmermann, R., Determann, J., and Rae, J.: Twenty-first-century warming of a large Antarctic ice-shelf cavity by a redirected coastal current, Nature, 485, 225, 2012.

Hindmarsh, R.: A numerical comparison of approximations to the Stokes equations used in ice sheet and glacier modeling, J. Geophys. Res., 109, https://doi.org/10.1029/2003JF000065, 2004.

Holland, P. R., Bracegirdle, T. J., Dutrieux, P., Jenkins, A., and Steig, E. J.: West Antarctic ice loss influenced by internal climate variability and anthropogenic forcing, Nature Geoscience, pp. 1–7, 2019.

Jenkins, A., Nicholls, K. W., and Corr, H. F. J.: Observation and parameterization of ablation at the base of Ronne Ice Shelf, Antarctica, J. Phys. Oceanogr., 40, 2298–2312, 2010.

Jenkins, A., Shoosmith, D., Dutrieux, P., Jacobs, S., Kim, T. W., Lee, S. H., Ha, H. K., and Stammerjohn, S.: West Antarctic Ice Sheet retreat in the Amundsen Sea driven by decadal oceanic variability, Nature Geosc., 11, 733–738, 2018.

Joughin, I., Smith, B. E., and Medley, B.: Marine ice sheet collapse potentially under way for the Thwaites Glacier Basin, West Antarctica, Science, 344, 735–738, https://doi.org/10.1126/science.1249055, 2014.

Jourdain, N. C., Asay-Davis, X., Hattermann, T., Straneo, F., Seroussi, H., Little, C. M., and Nowicki, S.: A protocol for calculating basal melt rates in the ISMIP6 Antarctic ice sheet projections, The Cryosphere Discussions, https://doi.org/https://doi.org/10.5194/tc-2019-277, in review.

Larour, E., Seroussi, H., Adhikari, S., Ivins, E., Caron, L., Morlighem, M., and Schlegel, N.: Slowdown in Antarctic mass loss from solid Earth and sea-level feedbacks, Science, 364, eaav7908, https://doi.org/10.1126/science.aav7908, 2019.

Leguy, G. R., Asay-Davis, X. S., and Lipscomb, W. H.: Parameterization of basal friction near grounding lines in a one-dimensional ice sheet model, The Cryosphere, 8, 1239–1259, https://doi.org/10.5194/tc-8-1239-2014, 2014.

Levermann, A., Winkelmann, R., Albrecht, T., Goelzer, H., Golledge, N. R., Greve, R., Huybrechts, P., Jordan, J., Leguy, G., Martin, D., Morlighem, M., Pattyn, F., Pollard, D., Quiquet, A., Rodehacke, C., Seroussi, H., Sutter, J., Zhang, T., Van Breedam, J., DeConto, R., Dumas, C., Garbe, J., Gudmundsson, G. H., Hoffman, M. J., Humbert, A., Kleiner, T., Lipscomb, W., Meinshausen, M., Ng, E., Perego, M., Price, S. F., Saito, F., Schlegel, N.-J., Sun, S., and van de Wal, R. S. W.: Projecting Antarctica's contribution to future sea level rise

https://doi.org/10.5194/tc-2019-334
Preprint. Discussion started: 14 January 2020

from basal ice-shelf melt using linear response functions of 16 ice sheet models (LARMIP-2), Earth System Dynamics Discussions, 2019, 1–63, https://doi.org/10.5194/esd-2019-23, 2019.

Lipscomb, W. H., Price, S. F., Hoffman, M. J., Leguy, G. R., Bennett, A. R., Bradley, S. L., Evans, K. J., Fyke, J. G., Kennedy, J. H., Perego, M., Ranken, D. M., Sacks, W. J., Salinger, A. G., Vargo, L. J., and Worley, P. H.: Description and evaluation of the Community Ice Sheet Model (CISM) v2.1, Geosci. Model Dev., 12, 387–424, https://doi.org/10.5194/gmd-12-387-2019, 2019.

Little, C. M., Gnanadesikan, A., and Oppenheimer, M.: How ice shelf morphology controls basal melting, J. Geophys. Res., 114, 2009.

Locarnini, R. A., Mishonov, A. V., Baranova, O. K., Boyer, T. P., Zweng, M. M., Garcia, H. E., Reagan, J. R., Seidov, D., Weathers, K. W., Paver, C. R., and Smolyar, I. V.: World Ocean Atlas 2018, Volume 1: Temperature, Tech. Rep. Atlas NESDIS 81, NOAA, https://data.nodc.noaa.gov/woa/WOA18/DOC/woa18_vol1.pdf, 2019.

MacAyeal, D. R.: Large-scale ice flow over a viscous basal sediment - Theory and application to Ice Stream B, Antarctica, J. Geophys. Res., 94, 4071–4087, 1989.

Mercer, J. H.: West Antarctic ice sheet and CO 2 greenhouse effect- A threat of disaster, Nature, 271, 321–325, 1978.

Morlighem, M., Rignot, E., Seroussi, H., Larour, E., Dhia, H. B., and Aubry, D.: A mass conservation approach for mapping glacier ice thickness, Geophys. Res. Lett., 38, L19503, https://doi.org/10.1029/2011GL048659, 2011.

Morlighem, M., Rignot, E., Binder, T., Blankenship, D., Drews, R., Eagles, G., Eisen, O., Ferraccioli, F., Forsberg, R., Fretwell, P., Goel, V., Greenbaum, J. S., Gudmundsson, H., Guo, J., Helm, V., Hofstede, C., Howat, I., Humbert, A., Jokat, W., Karlsson, N. B., Lee, W. S., Matsuoka, K., Millan, R., Mouginot, J., Paden, J., Pattyn, F., Roberts, J., Rosier, S., Ruppel, A., Seroussi, H., Smith, E. C., Steinhage, D., Sun, B., Broeke, M. R. v. d., Ommen, T. D. v., Wessem, M. v., and Young, D. A.: Deep glacial troughs and stabilizing ridges unveiled beneath the margins of the Antarctic ice sheet, Nature Geoscience, https://doi.org/10.1038/s41561-019-0510-8, 2019.

Mouginot, J., Scheuchl, B., and Rignot, E.: MEaSUREs Antarctic Boundaries for IPY 2007-2009 from Satellite Radar, Version 2, Tech. rep., Boulder, Colorado USA. NASA National Snow and Ice Data Center Distributed Active Archive Center, https://doi.org/10.5067/AXE4121732AD, https://nsidc.org/data/nsidc-0709/versions/2, 2017.

Naughten, K. A., Meissner, K. J., Galton-Fenzi, B. K., England, M. H., Timmermann, R., and Hellmer, H. H.: Future projections of Antarctic ice shelf melting based on CMIP5 scenarios, J. Climate, 31, 5243–5261, 2018.

Ng, F. and Conway, H.: Fast-flow signature in the stagnated Kamb Ice Stream, West Antarctica, Geology, 32, 481–484, https://doi.org/10.1130/G20317.1, 2004.

Nowicki, S., Payne, A., Goelzer, H., Seroussi, H., Lipscomb, W., Abe-Ouchi, A., Agosta, C., Alexander, P., Asay-Davis, X., Barthel, A., Bracegirdle, T., Cullather, R., Felikson, D., Fettweis, X., Gregory, J., Hatterman, T., Jourdai, N., Munneke, P. K., Larour, E., Little, C., Morlinghem, M., Nias, I., Shepherd, A., Simon, E., Slater, D., Smith, R., Straneo, F., Trusel, L., van den Broeke, M., and van de Wal, R.: Experimental protocol for sea level projections from ISMIP6 standalone ice sheet models, The Cryosphere, in review.

Nowicki, S. M. J., Payne, T., Larour, E., Seroussi, H., Goelzer, H., Lipscomb, W., Gregory, J., Abe-Ouchi, A., , and Shepherd, A.: Ice Sheet Model Intercomparison Project (ISMIP6) contribution to CMIP6, Geosci. Model Dev., 9, 4521–4545, https://doi.org/10.5194/gmd-9-4521-2016, 2016.

Pattyn, F.: A new three-dimensional higher-order thermomechanical ice sheet model: Basic sensitivity, ice stream development, and ice flow across subglacial lakes, J. Geophys. Res., 108, 2003.

Pattyn, F.: Role of transition zones in marine ice sheet dynamics, J. Geophys. Res., 111, F02 004, https://doi.org/10.1029/2005JF000394, 2006.

https://doi.org/10.5194/tc-2019-334
Preprint. Discussion started: 14 January 2020

Pattyn, F.: The paradigm shift in Antarctic ice sheet modelling, Nature Communications, 9, https://doi.org/10.1038/s41467-018-05003-z, 2018.

Pattyn, F., Perichon, L., Aschwanden, A., Breuer, B., de Smedt, B., Gagliardini, O., Gudmundsson, G. H., Hindmarsh, R. C. A., Hubbard, A., Johnson, J. V., Kleiner, T., Konovalov, Y., Martin, C., Payne, A. J., Pollard, D., Price, S., Rückamp, M., Saito, F., Souček, O., Sugiyama, S., and Zwinger, T.: Benchmark experiments for higher-order and full-Stokes ice sheet models (ISMIP—HOM), The Cryosphere, 2, 95–108, https://doi.org/10.5194/tc-2-95-2008, 2008.

Pattyn, F., Schoof, C., Perichon, L., Hindmarsh, R. C. A., Bueler, E., de Fleurian, B., Durand, G., Gagliardini, O., Gladstone, R., Goldberg, D., Gudmundsson, G. H., Huybrechts, P., Lee, V., Nick, F. M., Payne, A. J., Pollard, D., Rybak, O., Saito, F., and Vieli, A.: Results of the Marine Ice Sheet Model Intercomparison Project, MISMIP, The Cryosphere, 6, 573–588, https://doi.org/10.5194/tc-6-573-2012, 2012.

Pattyn, F., Perichon, L., Durand, G., Favier, L., Gagliardini, O., Hindmarsh, R. C., Zwinger, T., Albrecht, T., Cornford, S., Docquier, D., and et al.: Grounding-line migration in plan-view marine ice-sheet models: results of the ice2sea MISMIP3d intercomparison, J. Glaciol., 59, 410–422, https://doi.org/10.3189/2013JoG12J129, 2013.

Pimentel, S., Flowers, G. E., and Schoof, C. G.: A hydrologically coupled higher-order flow-band model of ice dynamics with a Coulomb friction sliding law, J. Geophys. Res., 115, 1–16, https://doi.org/10.1029/2009JF001621, 2010.

Pollard, D. and Deconto, R. M.: Modelling West Antarctic ice sheet growth and collapse through the past five million years, Nature, 458, 329–332, 2009.

Pollard, D. and DeConto, R. M.: Description of a hybrid ice sheet-shelf model, and application to Antarctica, Geoscientific Model Development, 5, 1273–1295, https://doi.org/10.5194/gmd-5-1273-2012, 2012.

Pollard, D. and DeConto, R. M.: Contribution of Antarctica to past and future sea-level rise, Nature, 531, 591–597, https://doi.org/10.1038/nature17145, 2016.

Pollard, D., DeConto, R. M., and Alley, R. B.: Potential Antarctic Ice Sheet retreat driven by hydrofracturing and ice cliff failure, Earth Planet. Sc. Lett., 412, 112–121, 2015.

Rignot, E., Mouginot, J., and Scheuchl, B.: Ice flow of the Antarctic Ice Sheet, Science, 333, 1427–1430, https://doi.org/10.1126/science.1208336, 2011.

Rignot, E., Jacobs, S., Mouginot, J., and Scheuchl, B.: Ice-shelf melting around Antarctica, Science, 341, 266–270, 2013.

Rignot, E., Mouginot, J., Morlighem, M., Seroussi, H., and Scheuchl, B.: Widespread, rapid grounding line retreat of Pine Island, Thwaites, Smith, and Kohler glaciers, West Antarctica, from 1992 to 2011, Geophys. Res. Lett., 41, 3502–3509, 2014.

Rignot, E., Mouginot, J., Scheuchl, B., van den Broeke, M., van Wessem, M. J., and Morlighem, M.: Four decades of Antarctic Ice Sheet mass balance from 1979–2017, Proceedings of the National Academy of Sciences, 116, 1095–1103, 2019.

Ritz, C., Edwards, T. L., Durand, G., Payne, A. J., Peyaud, V., and Hindmarsh, R. C. A.: Potential sea-level rise from Antarctic ice-sheet instability constrained by observations, Nature, 528, 115–118, 2015.

Rutt, I., Hagdorn, M., Hulton, N., and Payne, A.: The Glimmer community ice sheet model, J. Geophys. Res., 114, F02 004, 2009.

Schoof, C.: The effect of cavitation on glacier sliding, Proc. R. Soc. A, 461, 609–627, https://doi.org/10.1098/rspa.2004.1350, 2005.

Schoof, C.: Ice sheet grounding line dynamics: Steady states, stability, and hysteresis, J. Geophys. Res., 112, 2007.

Seroussi, H., Morlighem, M., Larour, E., Rignot, E., and Khazendar, A.: Hydrostatic grounding line parameterization in ice sheet models, The Cryosphere, 8, 2075–2087, https://doi.org/10.5194/tc-8-2075-2014, 2014.

Seroussi, H., Nakayama, Y., Larour, E., Menemenlis, D., Morlighem, M., Rignot, E., and Khazendar, A.: Continued retreat of Thwaites Glacier, West Antarctica, controlled by bed topography and ocean circulation, Geophysical Research Letters, 44, 6191–6199, 2017.

https://doi.org/10.5194/tc-2019-334
Preprint. Discussion started: 14 January 2020

Seroussi, H., Nowicki, S., Simon, E., Abe-Ouchi, A., Albrecht, T., Brondex, J., Cornford, S., Dumas, C., Gillet-Chaulet, F., Goelzer, H., Golledge, N. R., Gregory, J. M., Greve, R., Hoffman, M. J., Humbert, A., Huybrechts, P., Kleiner, T., Larour, E., Leguy, G., Lipscomb, W. H., Lowry, D., Mengel, M., Morlighem, M., Pattyn, F., Payne, A. J., Pollard, D., Price, S. F., Quiquet, A., Reerink, T. J., Reese, R., Rodehacke, C. B., Schlegel, N.-J., Shepherd, A., Sun, S., Sutter, J., Breedam, J. V., van de Wal, R. S. W., Winkelmann, R., and Zhang, T.: initMIP-Antarctica: an ice sheet model initialization experiment of ISMIP6, The Cryosphere, 13, 1441–1471, https://doi.org/10.5194/tc-13-1441-2019, 2019.

Seroussi, H., Nowicki, S., Payne, A. J., Goelzer, H., Lipscomb, W. H., Ouchi, A. A., Agosta, C., Albrecht, T., Asay-Davis, X., Barthel, A., Calov, R., Cullather, R., Dumas, C., Gladstone, R., Golledge, N., Gregory, J. M., Greve, R., Hatterman, T., Hoffman, M. J., Humbert, A., Huybrechts, P., Jourdain, N. C., Kleiner, T., Larour, E., Leguy, G. R., Lowry, D. P., Little, C. M., Morlighem, M., Pattyn, F., Pelle, T., Price, S. F., Quiquet, A., Reese, R., Schlegel, N.-J., Shepherd, A., Simon, E., Smith, R. S., Straneo, F., Sun, S., Trusel, L. D., Breedam, J. V., van de Wal, R. S. W., Winkelmann, R., Zhao, C., Zhang, T., , and Zwinger, T.: ISMIP6 Antarctica: a multi-model ensemble of the Antarctic ice sheet evolution over the 21st century, The Cryosphere, in review.

Shapiro, N. and Ritzwoller, M.: Inferring surface heat flux distributions guided by a global seismic model: particular application to Antarctica, Earth Planet. Sci. Lett., 223, 213–224, https://doi.org/10.1016/j.epsl.2004.04.011, 2004.

Shepherd, A., Ivins, E., Rignot, E., Smith, B., van den Broeke, M., Velicogna, I., Whitehouse, P., Briggs, K., Joughin, I., Krinner, G., Nowicki, S., Payne, T., Scambos, T., Schlegel, N., Geruo, A., Agosta, C., Ahlstrøm, A., Babonis, G., Barletta, V., Blazquez, A., Bonin, J., Csatho, B., Cullather, R., Felikson, D., Fettweis, X., Forsberg, R., Gallee, H., Gardner, A., Gilbert, L., Groh, A., Gunter, B., Hanna, E., Harig, C., Helm, V., Horvath, A., Horwath, M., Khan, S., Kjeldsen, K., Konrad, H., Langen, P., Lecavalier, B., Loomis, B., Luthcke, S., McMillan, M., Melini, D., Mernild, S., Mohajerani, Y., Moore, P., Mouginot, J., Moyano, G., Muir, A., Nagler, T., Nield, G., Nilsson, J., Noel, B., Otosaka, I., Pattle, M., Peltier, W., Nadege, P., Rietbroek, R., Rott, H., Sandberg-Sørensen, L., Sasgen, I., Save, H., Schrama, E., Schröder, L., Seo, K.-W., Simonsen, S., Slater, T., Spada, G., Sutterley, T., Talpe, M., Tarasov, L., van de Berg, W., van der Wal, W., van Wessem, M., Vishwakarma, B., Wiese, D., and Wouters, B.: Mass balance of the Antarctic ice sheet from 1992 to 2017, Nature, 558, 219–222, https://doi.org/10.1038/s41586-018-0179-y, 2018.

Stewart, A. L. and Thompson, A. F.: Eddy-mediated transport of warm Circumpolar Deep Water across the Antarctic Shelf Break, Geophys. Res. Lett., 42, 432–440, 2015.

Sun, S., Pattyn, F., Simon, E. G., Albrecht, T., Cornford, S., Calov, R., Dumas, C., Gillet-Chaulet, F., Goelzer, H., Golledge, N. R., Greve, R., Hoffman, M. J., Humbert, A., Kazmierczak, E., Kleiner, T., Leguy, G., Lazeroms, W. M. J., Lipscomb, W., Martin, D., Morlighem, M., Nowicki, S., Pollard, D., Price11, S., Quique, A., Seroussi, H., Schlemm, T., Sutter, J., van de Wal, R. S. W., Winkelmann, R., and Zhang, T.: Antarctic ice sheet response to sudden and sustained ice shelf collapse (ABUMIP), J. Glaciol., in review.

Thomas, R., Rignot, E., Casassa, G., Kanagaratnam, P., Acuña, C., Akins, T., Brecher, H., Frederick, E., Gogineni, P., Krabill, W., Manizade, S., Ramamoorthy, H., Rivera, A., Russell, R., Sonntag, J., Swift, R., Yungel, J., and Zwally, J.: Accelerated sea-level rise from West Antarctica, Science, 306, 255–258, https://doi.org/10.1126/science.1099650, 2004.

Timmermann, R. and Hellmer, H. H.: Southern Ocean warming and increased ice shelf basal melting in the twenty-first and twenty-second centuries based on coupled ice-ocean finite-element modelling, Ocean Dynamics, 63, 1011–1026, 2013.

Treasure, A. M., Roquet, F., Ansorge, I. J., Bester, M. N., Boehme, L., Bornemann, H., Charrassin, J.-B., Chevallier, D., Costa, D. P., Fedak, M. A., et al.: Marine mammals exploring the oceans pole to pole: a review of the MEOP consortium, Oceanography, 30, 132–138, 2017.

van Wessem, J. M., van de Berg, W. J., Noël, B. P. Y., van Meijgaard, E., Birnbaum, G., Jakobs, C. L., Krüger, K., Lenaerts, J. T. M., Lhermitte, S., Ligtenberg, S. R. M., Medley, B., Reijmer, C. H., van Tricht, K., Trusel, L. D., van Ulft, L. H., Wouters, B., Wuite, J.,

https://doi.org/10.5194/tc-2019-334
Preprint. Discussion started: 14 January 2020

and van den Broeke, M. R.: Modelling the climate and surface mass balance of polar ice sheets using RACMO2 – Part 2: Antarctica (1979–2016), The Cryosphere, 12, 1479–1498, https://doi.org/doi.org/10.5194/tc-12-1479-2018, 2018.

Weertman, J.: Stability of the Junction of an Ice Sheet and an Ice Shelf, Journal of Glaciology, 13, 3–11, https://doi.org/10.3189/s0022143000023327, 1974.

Zweng, M. M., Reagan, J. R., Seidov, D., Boyer, T. P., Locarnini, R., Garcia, H. E., Mishonov, A. V., Baranova, O. K., Weathers, K. W., Paver, C. R., and Smolyar, I. V.: World Ocean Atlas 2018, Volume 2: Salinity, Tech. Rep. Atlas NESDIS 82, NOAA, https://data.nodc.noaa.gov/woa/WOA18/DOC/woa18_vol2.pdf, 2019.